Empirical Evaluation of Short-Range WiFi Vessel-to-Shore Overwater Communications

Pedro M. d'Orey
CISTER Research Centre
Universidade do Porto, Portugal
ore@isep.ipp.pt

Miguel Gutiérrez Gaitán
Andres Bello University, Chile
CISTER Research Centre, Portugal
miguel.gutierrez@unab.cl

Pedro M. Santos
CISTER Research Centre
Polytechnic of Porto, Portugal
pss@isep.ipp.pt

Manuel Ribeiro
LSTS, Universidade do Porto
Porto, Portugal
maribeiro@fe.up.pt

João B. Sousa
LSTS, Universidade do Porto
Porto, Portugal
jtasso@fe.up.pt

Luís Almeida
CISTER Research Centre
Universidade do Porto, Portugal
lda@fe.up.pt

ABSTRACT

Unmanned vehicles used in ocean science, defense operations and commercial activities collect large amounts of data that is further processed onshore. For real-time information exchange, the wireless link between the unmanned vehicle and onshore devices must be reliable. In this work, we empirically evaluate a WiFi link between an autonomous underwater vehicle on the surface and an onshore device under real-world conditions. This work allowed i) collecting a large-scale realistic dataset and ii) identifying major factors impairing communication in such scenarios. The TX-RX antenna alignment, the operation mode (manual vs automatic) and varying reflecting surface induced by AUV mobility lead to sudden changes (e.g. *nulls*) in the received signal strength that can be larger than 20 dB. This study provides useful insights to the design of robust vessel-to-shore short-range communications.

CCS CONCEPTS

• **Networks** → **Ad hoc networks**; **Network performance analysis**.

KEYWORDS

ASV, AUV, owerwater communications, IEEE 802.11, mobility, vessel-to-shore, WiFi.

ACM Reference Format:
Pedro M. d'Orey, Miguel Gutiérrez Gaitán, Pedro M. Santos, Manuel Ribeiro, João B. Sousa, and Luís Almeida. 2022. Empirical Evaluation of Short-Range WiFi Vessel-to-Shore Overwater Communications. In *16th ACM Workshop on Wireless Network Testbeds, Experimental evaluation & CHaracterizatiion (WiNTECH'22), October 17, 2022, Sydney, NSW, Australia.* ACM, New York, NY, USA, 8 pages. https://doi.org/10.1145/3556564.3558240

WiNTECH'22, October 17, 2022, Sydney, NSW, Australia

ACM ISBN 978-1-4503-9527-4/22/10…$15.00
https://doi.org/10.1145/3556564.3558240

1 INTRODUCTION

Autonomous Underwater/Surface Vehicles (AUVs/ASVs) are key elements for characterizing and modeling the oceans [16] (e.g. seafloor mapping [9]), understanding natural phenomena (e.g. marine currents [1]), studying the impact of human activities (e.g. pollution), among many others. AUVs are also used for commercial activities (e.g. pipeline inspection [22]) or defense-related operations (e.g. surveillance). Usually, these vehicles perform pre-determined missions for collecting large amounts of (environmental) data (e.g. seawater salinity) in a given area of interest resorting to a plethora of sensors (e.g. sonar, camera, echo sounder).

The collected data is transmitted often in *real-time* - through terrestrial or satellite infrastructure - to backend datacenters for further processing or control. Cost constraints, operational restrictions and/or higher requirements on the timely delivery of information often require that data exchange is performed resorting to onshore rather than satellite communications. For terrestrial systems, the majority of the AUVs/ASVs use cellular [10][11] or unlicensed frequency bands (e.g. WiFi, LoRa [12] or TV white spaces [19]) for shore-based communications.

Overwater (shore-based) communications is impaired by a number of dynamic factors, such as tides [13] or waves [11]. Tides lead to variable antenna heights causing varying interference patterns between direct and (water) reflected paths resulting in considerable signal variations at the receiver. On the other hand, ocean dynamics (e.g. waves, wind, currents) can cause an inhomogeneous reflecting surface leading to variability in the water reflections, resulting in shadowing in agitated sea conditions. In addition, links can be blocked by other (moving) objects (e.g. boats [4]) or infrastructure. All these factors combined lead to widely fluctuating and unpredictable overwater communication links.

Related Work. Most of the works on studying large-scale signal propagation focus on long-range communications [5] that exhibit specific propagation effects (e.g. evaporation duct [21]), thus not being directly applicable to the near-shore case. On the other hand, recent work missed the impact of node mobility on the wireless link characteristics, focusing the evaluation solely on static scenarios (e.g. [12]). Thirdly, previous research often neglected the specificities of this type of vehicle. For instance, the very low antenna heights of AUV/ASV (i.e. comparable to the wavelength) can lead to additional or exacerbated propagation effects. Previous research on

other domains [18] showed that lower antenna height significantly impairs both small and large-scale propagation.

Contributions. In this work, we seek to characterize vessel-to-shore overwater short-range communications under realistic conditions, e.g. low AUV antenna height and typical node mobility. We collected large-scale measurements in a harbor setting using a autonomous vehicle equipped with commercial off-the-shelf (COTS) communication devices operating in the 2.4 GHz band, constituting an important tool for further research. Our main objective is to understand the impact of node mobility on the large-scale signal propagation for short-range overwater links. After assessing the large-scale link characteristics, we investigate the impact on the received signal strength of the *i*) travel direction, *ii*) TX-RX alignment and and *iii*) onshore antenna height, to provide insights into realistic link design and operation.

The remainder of the paper is organized as follow. Section 2 describes the experimental setup and the evaluation methodology. The empirical dataset is described in Section 3. The main results of the empirical evaluation study are presented in Section 4. Conclusions and future work are given in Section 5.

2 EXPERIMENTAL EVALUATION

2.1 Experimental setup

The experimental setup (Fig. 1) is composed of three main nodes that exchange/acquire mission information (e.g. telemetry, controls), namely *i*) Commercial Autonomous Underwater Vehicle (AUV) *Xplore-4* [1], *ii*) WiFi Access Point (AP) termed *Manta*[2], and *iii*) Dedicated Measurement equipment (DMU). In manual mode, the AUV was operated by a Remote Vehicle Controller (RVC), either consisting of a PC or a smartphone. The mobility of the RVC in the quay impaired its propagation conditions, thus being left out of this study. The length of the AUV is approximately 2 m.

Each node is equipped with two main components: a) *GNSS device* with external antenna for acquiring positioning and timing information and b) *IEEE 802.11 b/g/n radio* operating in the 2.4 GHz band equipped with external omni-directional antennas with different gains. Table 1 presents a summary of the specific COTS equipment used in the experiments. All radios were configured with the following settings: i) channel 3 with center frequency 2422 MHz, ii) 20 MHz bandwidth and iii) variable data rate. The AUV and AP transmit power have been set to 28 dBm and 25 dBm, respectively.

The AP antenna was secured to the computing device case, while the DMU antenna was attached to an adjustable tripod. The distance between the AP and DMU WiFi antenna base to the pier floor was 0.37 m, and 3.55/1.15 m for experiments I/II, respectively. The heights have been measured with a conventional tape with 0.1 cm precision. The AP and DMU were installed on-shore, thus their antenna heights w.r.t. the water surface varied due to the tide as detailed in Section 3.2. The AUV antenna height w.r.t. the water was 17 cm. The distance between the first floating element of the front/back of the AUV and its WiFi antenna is 127.5 cm and 33.5 cm, respectively.

[1] https://www.oceanscan-mst.com/
[2] The AUV and RVC associated with the AP at the beginning of the experiments.

Table 1: COTS Hardware used in the experiments

Node	GNSS Device	802.11 Radio	Ant. Gain
AUV	Ublox EVK-6	Ubiquity Picostation M2	5 dBi
AP	Ublox EVK-6	Ubiquity Bullet M2	8 dBi
DMU	Adafruit Ultimate GPS Breakout v3	Amiko WLN-880	5 dBi

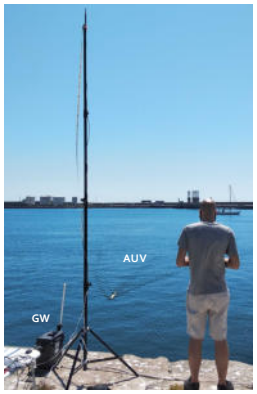

(a) Onshore setup (higher DMU ant. height for Exp. I).

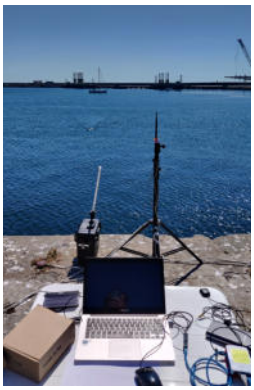

(b) Onshore setup (lower DMU ant. height for Exp. II).

(c) Autonomous Underwater Vehicle (AUV) *Xplore-4*

Figure 1: Experimental setup

2.2 Experimental Conditions

Measurement site. The measurement campaign was conducted in the Port of Leixões, Matosinhos, Portugal, during July 2021. The AP and DMU nodes were placed in close proximity (~1 m apart) on a concrete pier of the harbor at (41.185246, -8.704901) and (41.185273, -8.704882), respectively. The AUV operated in an enclosed area of the port.

AUV Mobility. The AUV was set to operate autonomously following a predetermined path defined by a set of waypoints. For safety reasons, the AUV was controlled manually near the quay. Fig. 2a shows the AUV trajectory (in blue) and the mean GPS positions of the AP and DMU. The AUV performed 15 equivalent round-trip missions starting from the quay and moving until ~100 m away (Fig. 2b), with Exp. I and Exp. II consisting of 7 and 6 round-trip missions, respectively. The AUV operated always on the surface at a low speed (1 m/s).

Propagation Conditions. Transmitter and receiver were predominantly in Line of Sight (LoS) conditions, except for rare occlusions caused by the quay and surrounding boats. The water was calm not

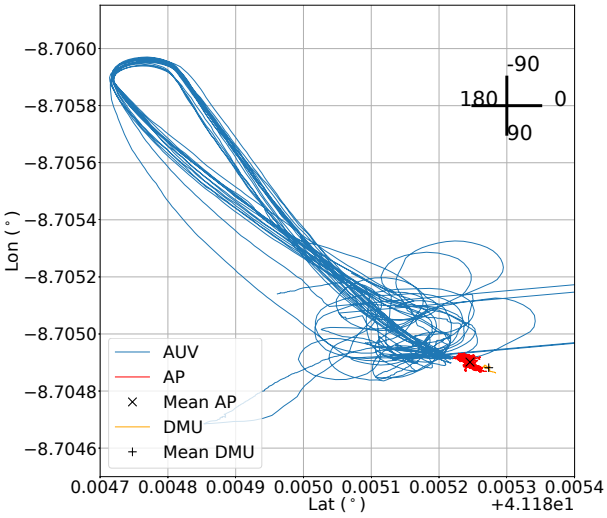

(a) AUV trajectory (in blue) and (mean) AP/DMU GPS positions. Reference Course Over Ground (COG) values are depicted in the upper right corner.

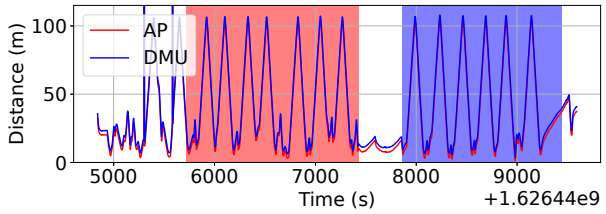

(b) Distance between AUV and AP/DMU for Exp. I (red area) with 7 round trips and Exp. II (blue area) with 6 round trips.

Figure 2: Node locations and AUV mobility patterns

causing shadowing or significant scattering [20]. We solely analyze AUV to AP/DMU transmissions assuming link reciprocity [17].

2.3 Measurement methodology

The AUV and AP devices measured the received signal strength with a 1 Hz rate using the manufacturer's software. On the other hand, to improve temporal resolution, the DMU radio was put in monitor mode, capturing all exchanged frames using the *tcpdump* application. Following, we processed the resulting file to extract: i) current system unix timestamp (t^i_{system}), ii) frame identifier, iii) frame (sub-)type, iv) frame length, v) TX's MAC address, vi) Received Signal Strength Indicator (RSSI) and vii) data rate.

Positioning and timing information was acquired with a frequency of 1 Hz. To overcome clock drifts, measurements from different nodes were aligned using the current GPS time (t^i_{GPS}) that was stored in a separate file along with the current node position and the system UNIX timestamp to determine the current clock offset ($\Delta = t^i_{system} - t^i_{GPS}$). The TX-RX node separation (distance) was determined by combining positioning and timing data and associated to the performance data (i.e. RSSI).

To study the influence of AUV mobility, we split manually the data into two types of segments using the TX-RX separation and

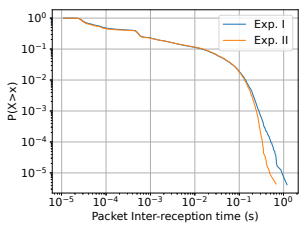

(a) Inter-Reception Time

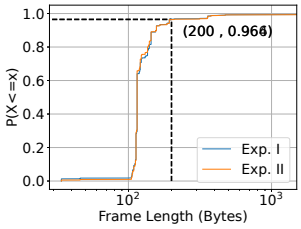

(b) Frame Size

Figure 3: Traffic Generation Statistics

AUV heading and velocity: *i*) *approach* (i.e. AUV approaching shore node) and *ii*) *recede* (i.e. AUV moving away from shore node).

3 DATASET CHARACTERIZATION

This section briefly describes and characterizes the collected dataset in more detail, focusing on the system dynamics (e.g. generated traffic) as well as on the dynamics of surrounding factors that impair the system performance (e.g. tides). The duration of experiments I and II was 28.5 and 26.4 min comprising 7 and 6 complete round-trip missions, respectively.

3.1 System Dynamics

Traffic generation. The AUV repeatedly executed its mission in the defined area moving perpendicular to the quay, maintaining its usual operational communication pattern, i.e., exchanging with the AP several types of data related to each of its sub-systems (e.g. networking, maneuvering or vehicle supervision). Due to differences in the underlying processes, the message generation frequency and packet sizes are distinct for different message types. In total, ~240 k/228 k frames were transmitted by the AUV (15.5/15.1% of all exchanged frames) during experiments I and II, respectively.

Fig. 3 gives a global view of the traffic generated by the AUV, showing an analysis of the packet generation rate and frame size. Since traffic acquisition was done by an external third-party (i.e. the AUV generated traffic was not logged), the exact generated traffic rate cannot be estimated. We approximate this metric using the Packet Inter-Reception time (PIR), i.e. time interval elapsed between the successful reception of two consecutive packets. Fig. 3a presents the inverse Cumulative Distribution Function (CDF) of the PIR metric for experiments I and II. The analysis shows that the PIR is below 10 ms in 90% of the cases, enabling also a fine-grained tracking of received signal power in time. The analysis also shows very similar PIR distributions for the two experiments, except for the larger tail in Exp. I for PIRs larger than 0.2 s.

Fig. 3b shows the CDF of the frame size revealing a relatively small frame with similar distributions for experiments I and II. In particular, ~96.7% of the frames are less than 200 Bytes long. Overall, the average frame size was 138/139 Bytes with a standard deviation of 125.6/130.6 Bytes for experiments I and II, respectively.

Mobility data. Fig. 4 shows the analysis of the AUV mobility (the mobility pattern was described in Section 2.2). The *Course of Ground* (*COG*) describes the actual direction of travel of the (autonomous) vehicle. Fig. 4a show that the range of COG angles is

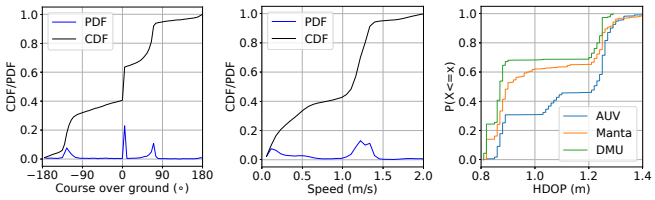

(a) COG (b) Speed (c) Horizontal DOP

Figure 4: Mobility data analysis, namely Course of Ground (COG), Speed and Horizontal Dilution of Precision (HDOP).

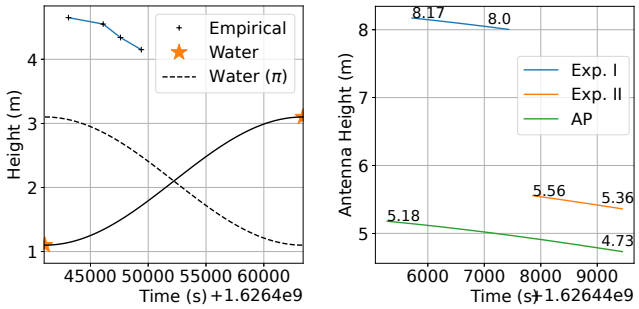

(a) Water level variations (b) Antenna Heights

Figure 5: Tide-induced Water Level Variations

not equally sampled and that there exist three main travel directions, i.e. approximately $\{-125°, 5°, 70°\}$. The unequal sampling of the COG range arises from the i) manual maneuvering of the AUV when in proximity to the quay and ii) initial objective of the experiments, which was to assess the impact of different onshore antenna heights on the performance of the communication link. Fig. 4b shows the Probability/Cumulative Density Function (PDF/CDF) of the AUV speed. The main mode of the distribution is slightly above the prescribed mission speed of 1 m/s due to water currents.

Nodes resort to GPS receivers to acquire position and time, which in turn is used to compute the distance between AUV and onshore nodes. For obtaining reliable (link quality) results, the precision of positioning data should be high. Fig. 4c presents one of the most popular positioning precision metrics termed Horizontal Dilution of Precision (HDOP). The results show that for all setups the HDOP varies between 0.8 and approximately 1.4 m, which is considered acceptable given the low vehicle speed ($\approx$ 1.25 m/s) and that typical bin sizes for link quality evaluations are larger than 10 m. As expected, the HDOP value is higher for the mobile AUV value. Due to favorable conditions (e.g. open sky), all setups have on average 10 visible satellites, which explains the low HDOP.

3.2 Environmental Dynamics

The onshore nodes' antenna heights w.r.t. the water surface varied during the experiments due to the recurrent rise and fall of the sea level (i.e. tides). The sea level in large bodies of water is determined in great measure by the varying gravitational forces of both the Moon and the Sun, and the rotation of the Earth [14]. Tides are also influenced by astronomical (e.g. lunar orbit) and meteorological factors (e.g. wind). Water level variations in open waters are typically described by a linear combination of sinusoidal terms.

Fig. 5a shows publicly available tidal data[3] describing water level variations for the measurement site (Leixões, Portugal) during half tidal cycle on July 16, 2021. We approximate the tidal dynamics resorting to a simple sinusoidal model [in black] and plot the same data with a phase shift of π [in dashed black] for comparison with empirical data. The empirical measurements of the distance between the pier floor and the current water level are also depicted [in blue]. This height decreases during the experiments due to the rise of the water level during the flooding period of the tidal cycle. Comparing the later empirical measurements and the output of the tidal model, we observe very well aligned trends, demonstrating the feasibility to model the phenomena with small error magnitudes, just using an offset k ($\approx$1.645 m).

Fig. 5b shows the antenna heights w.r.t. the water surface during the measurement campaign. The AP antenna height varied within [5.18, 4.73] m (45 cm). The DMU antenna height varied within [8.17, 8.0] m (17 cm) and within [5.56, 5.36] m (20 cm) for experiments I and II, respectively. Despite both experiments having similar duration, the water level variations are slightly more pronounced in Exp. II due to higher flooding velocities in that part of the tidal cycle. Note also that previous work [7] has shown that centimeter-level differences in antenna height can have a significant impact on the channel characteristics.

4 RESULTS

In this work, we aim at characterizing large-scale signal fluctuations of shore-to-vessel communication links under realistic AUV/ASV mobility. Furthermore, we aim at assessing how the system performance is dynamically impaired by the node mobility, surrounding propagation environment, and TX-RX alignment.

4.1 Aggregated results

Fig. 6 depicts the RSSI as a function of the TX-RX separation for the three cases (AP, DMU exp. I and DMU exp II). For all cases (Fig. 6a), as expected, the RSSI decreases *non-monotonically* with increasing distance, with observable dips in received power for certain relatively short TX-RX separations (*interference region*) but becoming monotonic after a certain distance (*break-point distance*). For instance, the received power diminishes by almost 10 dB for a TX-RX separation of approximately 17 m for the AP setup; note that the magnitude of the drop is not so pronounced for the DMU setup. These variations in received signal strength mainly arise from the constructive or destructive interference between the LOS and water-reflected paths that have different lengths. This constructive/destructive interference patterns are often modelled using the two-ray propagation model [3, 8]. The raw RSSI data presented in Figs. 6b, 6c and 6d makes these sudden signal variations even more evident. As expected, the number and location of these dips varies for different configurations due to different antenna heights w.r.t. the water surface, which changes the path length for the water-reflected ray and consequently creates different interference patterns.

[3] http://www.tabuademares.com

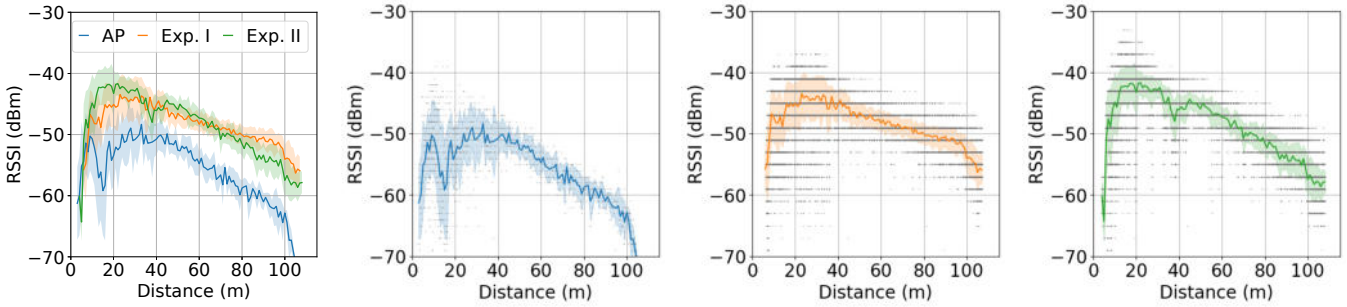

(a) All (b) AP (c) DMU Exp. I (d) DMU Exp. II

Figure 6: RSSI as a function of TX-RX separation. Each tendency line [shaded area] is the mean RSSI [standard deviation above/below the mean RSSI] for the given distance bin. The points in (b), (c) and (d) represent raw RSSI measurements for the AP and DMU experiments I and II, respectively.

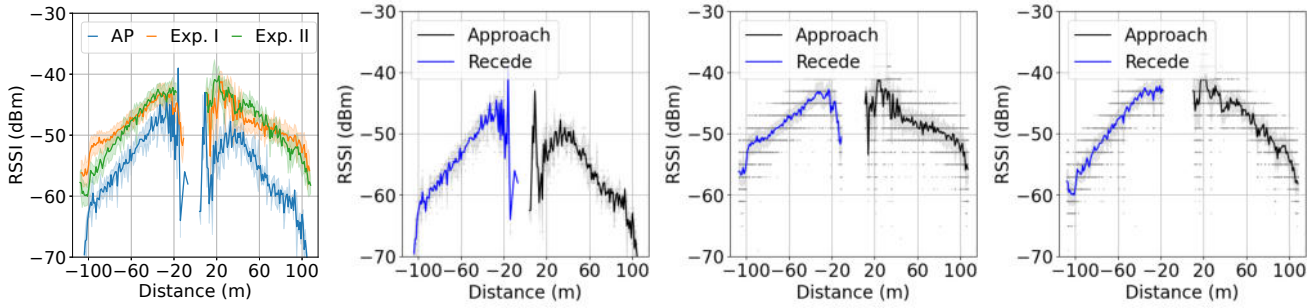

(a) All (b) AP (c) DMU Exp. I (d) DMU Exp. II

Figure 7: RSSI for *approach* and *recede* travel directions. Each tendency line [shaded area] in (a), (b), (c) and (d) is the mean RSSI [standard deviation above/below the mean RSSI] for the given distance bin and travel direction. The points in (b), (c) and (d) represent raw RSSI measurements for each configuration.

To analyze the variability of the RSSI for a given TX-RX separation bin, we resort to the average and the bounds of the standard deviation metric. The average standard deviation for all bins is 3.024, 2.374 and 2.309 for the AP, DMU exp. I and DMU exp. II setups, respectively. On the other hand the minimum and maximum RSSI standard deviation values considering all bins are [0.408, 9.033], [1.139, 5.934] and [1.079, 6.317] for the same three cases, respectively. The results show that the *i*) *AP* setup exhibits larger received signal variations (e.g. due to more pronounced null) and *ii*) variations for the experiments I and II of *DMU* setup are similar.

Impact of Antenna Heights. In the deployment of shore-to-vessel communication systems, the common practice is to install onshore node antennas at the highest position the setup allows. In our experiments we accommodate three antenna height ranges (Fig. 5b) to represent different settings. For the DMU setup, the results in Fig. 6a provide initial evidence that the highest antenna position often fails in providing the best link quality, as alluded in previous studies [6, 8]. Note also the overlap between the shaded areas for experiments I and II. We argue that this occurs for several reasons, namely the *i*) low AUV antenna height and *ii*) short TX-RX distances (falling within the self-interference zone), which can be explained by the geometrical basis of the two-ray model.

4.2 Impact of Travel Direction

To understand the influence of the AUV travel direction w.r.t. to the shore, we classified the collected data into *approach* and *recede* travel directions. For a fair comparison, we solely consider the data segments where the vehicle was operating autonomously.

Fig. 7 shows the RSSI as a function of distance split per travel direction. As expected, the RSSI as a function of the TX-RX separation (Fig. 7a) shows similar trends to the ones given in Fig. 6a. Now comparing these trends for a given setup (e.g. Fig. 7b or 7c or 7c), we

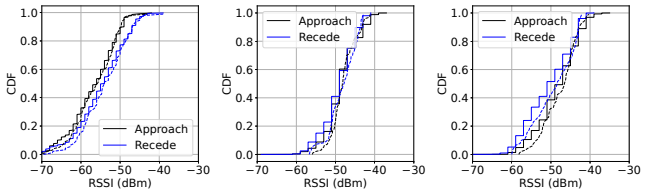

(a) AP (b) DMU Exp. I (c) DMU Exp. II

Figure 8: RSSI CDF of the raw (full line) and aggregated (dashed line) data for the three configurations.

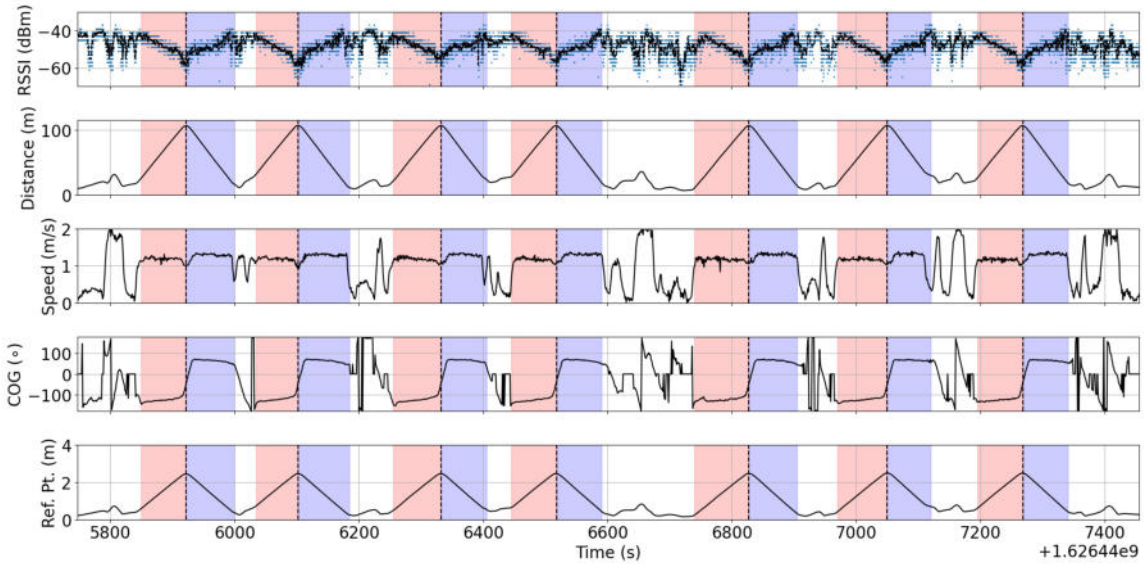

Figure 9: Aggregated and Raw RSSI as a function of time for DMU Exp. I, including temporal variation of the AUV-shore distance, AUV speed, Course over Ground (COG) and reflection point distance w.r.t. to the AUV WiFi antenna. The segments corresponding to the *recede*/*approach* travel directions are depicted as bands in orange/blue.

observe (substantial) differences between both travel directions in terms of magnitude and location of the dips. These differences are specially evident for the *AP* setup. While in the *AP* setup the *recede* direction shows higher RSSI (Fig. 8a), the received signal level is larger for the *approach* direction in the *DMU exp. II* setup (Fig. 8c). In the *DMU exp. I* setup the distributions of the RSSI for both travel directions are similar. In this context, we apply the Cramér–von Mises test [15] to statistically compare the distributions of the two directions in each setup considering a significance level of 5%. The null hypothesis for this criterion states the equality of distributions, i.e., observed samples are drawn from the same distribution. The results given in Table 2 show that the null hypothesis can only be rejected for the *AP* setup, i.e., samples are not drawn from the same distribution.

Several reasons can cause these discrepancies between *approach* and *recede* communication links, namely *i*) non-uniform radiation pattern of the quasi omni-directional antennas, *ii*) antenna tilting causing different TX-RX alignment due to the tilting of the AUV arising from its propulsion, among others.

Impact of Antenna Heights. For the DMU setup, the results corroborate previous findings that provide similar results in terms of RSSI for both travel directions despite the different antenna heights of experiments I and II.

Table 2: Cramér–von Mises test between travel directions using aggregated data considering a significance level of 0.05.

Setup	Statistic	p-value	Result
AP	0.78323	0.00799	Reject
DMU Exp. I	0.24500	0.19578	Not Reject
DMU EXp. II	0.39260	0.07571	Not Reject

4.3 Impact of Node Mobility

Fig. 9 shows raw and aggregated RSSI as a function of time for DMU Exp. I [4] alongside with mobility related metrics, namely TX-RX separation, AUV speed and Course over Ground (COG). These results exhibit a clear impact of the AUV mobility pattern on the received signal strength. Specifically, despite the use of omni-directional antennas and for similar TX-RX separations, (fast) AUV turns (shown by the COG metric) lead to clearer dips in the RSSI pattern. These dips, which can impair communication between the AUV and the shore node (e.g. link break or modulation adaptation), can be larger than 20 dB and are specially evident when the vehicle was being operated manually, i.e. outside the orange and blue bands corresponding to autonomous operation for the *recede* and *approach* travel directions, respectively.

Under autonomous operation, RSSI dips (not explained by destructive interference) occur also when the vehicle COG is approximately zero, i.e. the AUV is perpendicular to the shore node. Nevertheless, these dips are less pronounced when comparing to the ones occurring during manual operation. We argue that this type of RSSI dips are due to TX-RX antenna misalignment that cause a degradation of transmitted/received signal given non-isotropic features in radiation patterns of these nodes; other effects (e.g. AUV structure) might also influence the effective radiation patterns.

Sudden signal variations are also observed at the end of the *approach* travel direction despite the constant AUV COG. We argue that this effect might be attributed to a change in the reflection surface of the secondary ray. The bottom image of Fig. 9 depicts the position of the reflection point w.r.t. to the AUV WiFi antenna. The results show that the reflection point lies within 2 m of the WiFi antenna. While for the majority of the *approach* and *recede*

[4] We omit the results for other configurations due to space constraints.

travel directions the reflection point lies in the water close to the AUV, extreme cases for the *approach* direction, only, may place the reflection point on the AUV body itself. Note that the WiFi antenna is placed towards the back part of the AUV as show in Fig. 1c, thus it does not affect the *receding* direction. Please recall that the distance between the first floating element of the front/back of the AUV and its WiFi antenna is 127.5 cm and 33.5 cm, respectively. The different characteristics of the materials that reflect the secondary ray (i.e. water and metallic AUV) will lead to changes in the reflection coefficient and consequently in the destructive/constructive interference pattern.

4.4 Impact on Data Rate

To determine the instantaneous channel capacity, we extract the negotiated IEEE 802.11 data rate from each frame contained in the experimental packet capture files of experiments I and II. Note that the devices implemented a proprietary rate adaptation scheme [2]. Considering a bandwidth of 20 MHz and a single spatial stream, the data rates of an IEEE 802.11 b/g/n network vary between 1 Mbps and 65 Mbps using different modulation types and coding schemes. Fig. 10 depicts the relative frequency of each data rate for experiments I and II. For both experiments, the results demonstrate that the data rates are equal or lager than 26 Mbps in about 95% of the occasions given the favorable propagation conditions (e.g. LoS, no obstacles), with the most frequent data rate being 58.5 Mbps. As expected, the distributions of the data rates for experiments I and II are similar given the comparable conditions (e.g. in terms of RSSI as shown in Section 4.1).

Fig. 11 depicts the negotiated data rates as a function of distance for experiments I and II. The results given in Fig.11a demonstrate the adaptation of the current bit data in accordance with the current channel conditions (e.g. the data rate is decreased in more challenging propagation conditions). This fact is corroborate by Fig. 12 that analyzes the relation between negotiated data rate and the corresponding signal strength, with lower signal strenght values corresponding to higher proportions of lower modulation and coding schemes. For instance, in the region where the AUV performs the U-turn ($d \approx 100$ m) that has more challenging propagation conditions as shown in previous sections, the rate adaptation algorithm dramatically reduces the (average) available data rate in experiments I (Fig 11b) and II (Fig 11c).

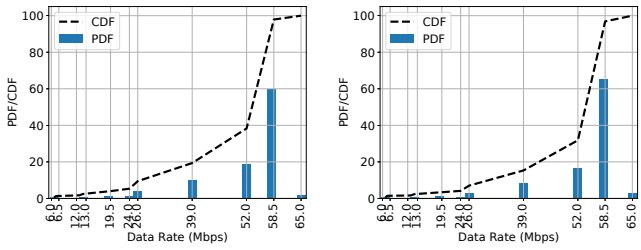

(a) Exp. II (b) Exp. II

Figure 10: Frequency of negotiated IEEE 802.11 b/g/n data rates for experiments I and II.

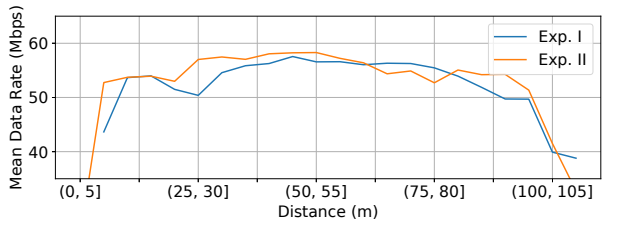

(a) Mean (Exp. I and II)

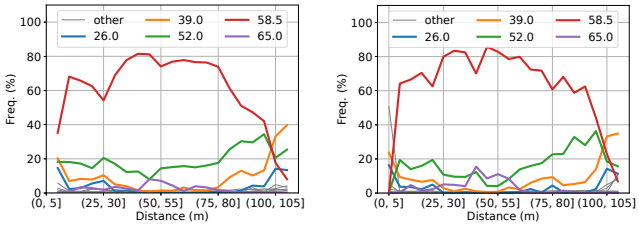

(b) Frequency (Exp. I) (c) Frequency (Exp. II)

Figure 11: Negotiated data rates as a function of distance for experiments I and II. We consider a bin size of 5 m.

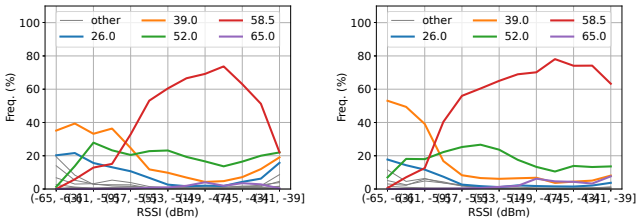

(a) Exp. II (b) Exp. II

Figure 12: Relative frequency of negotiated data rates as a function of the RSSI for experiments I and II. We consider a bin size of 2 dB.

Fig. 11a also demonstrates that the most favorable region for data transmission is not necessarily within short TX-RX distances and that instead the region after the *interference* zone (i.e. distances between approximately 35 and 75 m) should be considered for data offloading.

4.5 Discussion

We observed the occurrence of variations in received signal strength that can be assigned to constructive or destructive interference between the LOS and water-reflected paths. Such results provide further support that the two-ray propagation model accurately describes observed behaviour in vessel-to-shore scenarios. In addition, we observed that the very low AUV antenna height w.r.t. the water (comparable to the wavelength) creates situations in which the reflection is on the AUV body leading to significant signal strength variations when comparing to the reflection of the secondary ray on the water.

We also observed divergences between both travel directions regarding RSSI magnitude and location of dips. This was particularly evident for the AP setup, in which it was possible to establish that samples acquired in the two directions come from different distributions. Also interestingly, the largest RSSI values for the *recede* direction were observed by the AP setup, and for the *approach* direction for the DMU Exp. II setup. In turn, dips in RSSI were specially evident when the vehicle was being operated manually, especially at turning points. This implies that, even when occurring at the smallest distance, turning occasions do not constitute the best intervals for data transfer between vessel and shore.

Such results show that the travel direction and particular maneuvers may have a relevant and noticeable impact in the performance of the wireless communication. Equipped with the above information, transmitted data volumes can be maximized (while energy efficiency is improved) by limiting data transfer to windows in which favourable conditions occur, and refraining or withholding data if such conditions are not met. Taking a step further, AUV paths themselves can be designed in a way that maximizes favourable conditions, so that relevant information can be transmitted reliably and throughout a large portion of a mission.

To conclude, AUV operators working in this scenario type should consider *simultaneously* the following set of parameters for the design of WiFi vessel-to-shore links, namely *i*) access point antenna height (e.g. higher might not be better), *ii*) travel direction (e.g. a given travel direction might present more favorable propagation conditions), *iii*) TX-RX alignment (e.g. turning and manual operation might impair propagation conditions) and *iv*) TX-RX separation (e.g. degraded conditions in the interference zone).

5 CONCLUSIONS

We studied the performance of vessel to near-shore communication links under realistic conditions. The results have shown that node mobility in all of its dimensions (e.g. turning angle) can significantly impair link quality with variations larger than 20 dB. This study provides initial directions for the design and operation of wireless links under these challenging operating conditions.

As future work, we intend to characterize the radiation patterns of the AUV-antenna set to use as input for a new, improved two-ray propagation model. On the other hand, we plan to further evaluate this communication link under more adverse sea conditions and considering different configurations. After performing new measurement, we shall also study the impact of the observed signal strength variations on higher network layer metrics (e.g. latency). As end goal, we seek to provide end-users with novel and featured tools to aid the design of robust wireless communication for AUV/USV-like vessels data-transfer operations at near-shore.

ACKNOWLEDGMENTS

This work was partially supported by National Funds through FCT/MCTES (Portuguese Foundation for Science and Technology), within the CISTER Unit(UIDP/UIDB/04234/2020), and by FCT and the ESF (European Social Fund) through the Regional Operational Programme (ROP) Norte 2020, under PhD grant 2020.06685.BD.

REFERENCES

[1] Benedetto Allotta, Riccardo Costanzi, Francesco Fanelli, Niccolò Monni, Libero Paolucci, and Alessandro Ridolfi. 2017. Sea currents estimation during AUV navigation using Unscented Kalman Filter. *IFAC World Congress* 50, 1 (2017), 13668–13673.

[2] Saad Biaz and Shaoen Wu. 2008. Rate adaptation algorithms for IEEE 802.11 networks: A survey and comparison. In *IEEE Symposium on Computers and Communications*. IEEE, Marrakech, Morocco, 130–136.

[3] Ghassan Dahman, Denis Couillard, Marie-Eve Grandmaison, Gwenael Poitau, and Francois Gagnon. 2019. Improved 2-Ray Model for Overwater Propagation Channels: Modeling the Instantaneous Variations in the Received Signal Strength. *IEEE Wireless Communications Letters* 8, 3 (2019), 865–868.

[4] Riadh Essaadali, Ammar Kouki, Francois Gagnon, Denis Couillard, and Marie-Eve Grandmaison. 2015. Overwater point-to-multipoint radio pathloss characterization and modeling. In *IEEE Wireless Communications and Networking Conference (WCNC)*. IEEE, Istanbul, Turkey, 195–200.

[5] N. Fuke, K. Sugiyama, and H. Shinonaga. 2003. Long-range oversea wireless network using 2.4 GHz wireless LAN installation and performance. In *Int. Conf. on Computer Communications and Networks*. IEEE, Dallas, USA, 351–356.

[6] Miguel Gutiérrez Gaitán, Pedro M Santos, Luis R Pinto, and Luís Almeida. 2020. Optimal antenna-height design for improved capacity on over-water radio links affected by tides. In *Global OCEANS 2020: Singapore–US Gulf Coast*. IEEE, Biloxi, MS, USA, 1–7.

[7] Miguel Gutiérrez Gaitán, Pedro M. d'Orey, Pedro M. Santos, Manuel Ribeiro, Luís Pinto, Luís Almeida, and J. Borges De Sousa. 2021. Wireless radio link design to improve near-shore communication with surface nodes on tidal waters. In *IEEE OCEANS 2021*. IEEE, San Diego, USA, 1–8.

[8] Miguel Gutiérrez Gaitán, Pedro M. Santos, Luis R. Pinto, and Luis Almeida. 2020. Experimental evaluation of the two-ray model for near-shore WiFi-based network systems design. In *IEEE Vehicular Technology Conference*. IEEE, Antwerp, Belgium, 1–3.

[9] Emir Cem Gezer, Lin Zhao, Jordan Beason, and Mingxi Zhou. 2021. Towards seafloor mapping using an affordable micro-UUV. In *IEEE OCEANS*. IEEE, San Diego, USA, 1–5.

[10] Sanghai Guan, Jingjing Wang, Chunxiao Jiang, Ruiyang Duan, Yong Ren, and Tony Q. S. Quek. 2021. MagicNet: The Maritime Giant Cellular Network. *IEEE Communications Magazine* 59, 3 (2021), 117–123.

[11] Yiming Huo, Xiaodai Dong, and Scott Beatty. 2020. Cellular Communications in Ocean Waves for Maritime Internet of Things. *IEEE Internet of Things Journal* 7, 10 (2020), 9965–9979.

[12] Ruinan Li Li, Xiaolong Zheng, Yuting Wang, Liang Liu, and Huadong Ma. 2022. PolarScheduler: Dynamic Transmission Control for Floating LoRa Networks. In *IEEE INFOCOM*. IEEE, virtual, 550–559.

[13] Alex Macmillan, Mahesh K. Marina, and Jhair Tocancipa Triana. 2010. Slow Frequency Hopping for Mitigating Tidal Fading on Rural Long Distance Over-Water Wireless Links. In *IEEE Conference on Computer Communications Workshops*. IEEE, San Diego, USA, 1–5.

[14] David Pugh and Philip Woodworth. 2014. *Sea-level science: understanding tides, surges, tsunamis and mean sea-level changes*. Cambridge Uni. Press, Cambridge, United Kingdom.

[15] Jean-François Quessy and François Éthier. 2012. Cramér–von Mises and characteristic function tests for the two and k-sample problems with dependent data. *Computational Statistics & Data Analysis* 56, 6 (2012), 2097–2111.

[16] Jean-François Quessy and François Éthier. 2022. Coordinated Robotic Exploration of Dynamic Open Ocean Phenomena. *Field Robotics* 2 (2022), 843–871.

[17] Ehab Salahat, Ahmed Kulaib, Nazar Ali, and Raed Shubair. 2017. Exploring symmetry in wireless propagation channels. In *European Conference on Networks and Communications (EuCNC)*. IEEE, Oulu, Finland, 1–6.

[18] Devin P. Smith, Geoffrey G. Messier, and Michael W. Wasson. 2016. Boreal Forest Low Antenna Height Propagation Measurements. *IEEE Transactions on Antennas and Propagation* 64, 9 (2016), 4004–4011.

[19] Filipe B Teixeira, Tiago Oliveira, Mário Lopes, José Ruela, Rui Campos, and Manuel Ricardo. 2016. Tethered balloons and TV white spaces: A solution for real-time marine data transfer at remote ocean areas. In *IEEE Third Underwater Communications and Networking Conference (UComms)*. IEEE, Lerici, Italy, 1–5.

[20] Wei Wang, Gerald Hoerack, Thomas Jost, Ronald Raulefs, Michael Walter, and Uwe-Carsten Fiebig. 2015. Propagation channel at 5.2 GHz in Baltic sea with focus on scattering phenomena. In *European Conference on Antennas and Propagation (EuCAP)*. IEEE, Lisbon, Portugal, 1–5.

[21] Khurram Shabih Zaidi, Varun Jeoti, Micheal Drieberg, Azlan Awang, and Asif Iqbal. 2018. Fading Characteristics in Evaporation Duct: Fade Margin for a Wireless Link in the South China Sea. *IEEE Access* 6 (2018), 11038–11045.

[22] Hongwei Zhang, Shitong Zhang, Yanhui Wang, Yuhong Liu, Yanan Yang, Tian Zhou, and Hongyu Bian. 2021. Subsea pipeline leak inspection by autonomous underwater vehicle. *Applied Ocean Research* 107 (2021), 102321.